

# Infrared photon echo signatures of hydrogen bond connectivity in the cyclic decapeptide antamanide

Andrew M. Moran, Seung-Min Park, and Shaul Mukamel<sup>a)</sup>

Departments of Chemistry and Physics and Astronomy University of Rochester, Rochester, New York 14627-0216

(Received 7 January 2003; accepted 11 March 2003)

Distinct hydrogen bonding patterns are predicted in the amide I and amide A vibrational bands of four dominant conformations of antamanide using anharmonic vibrational Hamiltonians constructed at the DFT and AM1 levels. We show how these conformations may be distinguished using coherent three pulse infrared measurements with several pulse polarization configurations in the amide I region. The amide A hydrogen bonded N–H stretching modes are highly localized and have conformation-dependent frequencies, but their anharmonicities are insensitive to local structure at the hydrogen bond distances in antamanide. © 2003 American Institute of Physics.

[DOI: 10.1063/1.1571527]

## I. INTRODUCTION

The cyclic decapeptide antamanide (<sup>-1</sup>Val-<sup>-2</sup>Pro-<sup>-3</sup>Pro-<sup>-4</sup>Ala-<sup>-5</sup>Phe-<sup>-6</sup>Phe-<sup>-7</sup>Pro-<sup>-8</sup>Pro-<sup>-9</sup>Phe-<sup>-10</sup>Phe-) (Fig. 1) is a small oligopeptide which had served as a benchmark model system in the two-dimensional nuclear magnetic resonance (2D NMR) studies of protein secondary structure.<sup>1–8</sup> It has also been the subject of extensive molecular dynamics (MD) simulations (see Ref. 6 and references therein). Antamanide prevents the inhibition of depolymerization of F-actin and G-actin in the liver cell membranes of mammals, caused by the poisonous phalloidins that occur in the mushroom *Amanita 17a phalloides*.<sup>9</sup> It is found in small quantities in the same mushroom.

Antamanide has ten peptide bonds but only six amide hydrogens that can participate in the intramolecular hydrogen bonding network<sup>1,10</sup> since the four proline residues possess no amide hydrogens. Both one-dimensional (1D) NMR<sup>11</sup> and ultrasonic absorption measurements<sup>12</sup> in solution suggest that multiple conformations interchange on the microsecond time scale. More recent 2D NMR relaxation measurements in the rotating frame and homo- and heteronuclear coupling constant determinations have been used to characterize its dynamic properties; evidence for a  $\sim 25 \mu\text{s}$  conformational exchange process with an activation energy of  $20 \text{ kJ mol}^{-1}$  at 320 K was obtained.<sup>1</sup> These  $T_{1\rho}$  measurements are consistent with a rapid rearrangement of the hydrogen bonding pattern at <sup>1</sup>Val HN and <sup>6</sup>Phe HN, and concomitant changes in the local backbone dihedral angles. The two most probable dynamic-exchange pairs were identified; these are known as the *syn*-pair (E116 and G129 of Fig. 2) and the *anti*-pair (A128 and G193 of Fig. 2), because of *syn*- and *anti*-correlated dihedral angle changes at <sup>1</sup>Val HN and <sup>6</sup>Phe HN.<sup>1</sup> However, Blackledge *et al.*<sup>1</sup> pointed out that their best fit with experiment was not sufficient to exclude additional pair structures. Further measurements are thus neces-

sary in order to characterize the ensemble of possible structures in more detail.

Our aim in this work is to explore possible signatures of the hydrogen bonding networks of antamanide in coherent infrared multiple pulse signals. Such experiments are complementary to NMR since they can monitor structural variations on an ultrafast (femtosecond) time scale by watching them through a different window than NMR: fluctuations of various parameters such as transition dipole moments and frequencies. We focus on the amide I and amide A modes because they have well-defined internal coordinate compositions<sup>13,14</sup> and are amenable to an excitonic description.<sup>15,16</sup> Excitonic models allow to parametrize Hamiltonians of extended systems using information obtained from high-level calculations on smaller model molecules.<sup>17,18</sup> Excitonic modeling is necessary for the present simulations because antamanide is too large for density functional theory (DFT) calculations of the entire peptide.

We have constructed anharmonic vibrational Hamiltonians for four conformations of antamanide using a procedure recently developed and applied to identify spectroscopic signatures that distinguish  $\alpha$ - and  $3_{10}$ -helices<sup>18</sup> in a 15-unit polyalanine oligomer. DFT calculations of *trans*-N-methylacetamide (NMA) dimers configured to represent the two helical motifs showed that the amide A anharmonicity is highly sensitive to local structure. Specifically, the quartic anharmonicity was calculated to be  $45.4$  and  $52.9 \text{ cm}^{-1}$  for the  $3_{10}$  and  $\alpha$ -helices, respectively. <sup>13</sup>C isotopic derivatives that optimally reveal the local helical structures were identified for distinguishing the two conformations. A similar parametrization scheme has been applied recently to the amide I modes of flavodoxin and myoglobin; *ab initio* derived bilinear coupling constants were used to generate part of the Hessian matrices for these proteins.<sup>17</sup>

Our algorithm for calculating anharmonic force fields<sup>19</sup> yields energy levels that are consistent with both experimental measurements<sup>20</sup> and with an alternative *ab initio* theoret-

<sup>a)</sup>Electronic mail: mukamel@chem.rochester.edu

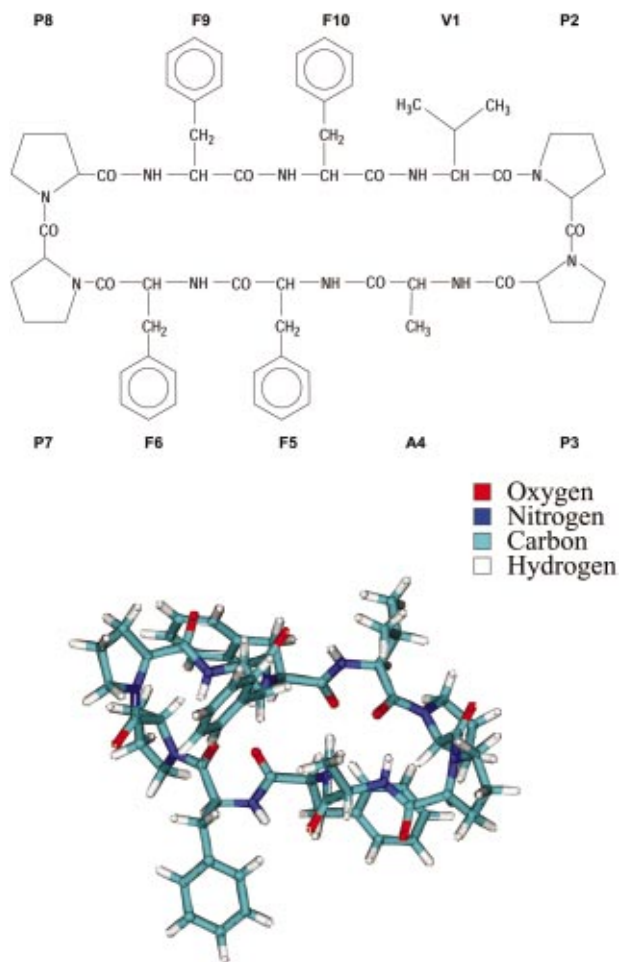


FIG. 1. (Color) Three-dimensional image of the lowest energy conformer (A) of antamanide found in this work using the semiempirical AM1 Hamiltonian.

ical method for computing anharmonic effects on fundamental vibrational frequencies.<sup>21,22</sup> The vibrational self-consistent field algorithm<sup>21</sup> was recently applied to NMA,<sup>22</sup> anharmonic contributions were found to shift the fundamental amide I and A frequencies by 29 and 229  $\text{cm}^{-1}$ , whereas shifts of 40.5 and 186.4  $\text{cm}^{-1}$  were found using our methodology<sup>19</sup> (we reported fundamental frequencies calculated for an anharmonic potential of NMA in Ref. 18). This agreement supports our assumption that vibrational amplitude of the amide A and I modes are predominantly localized on one and four internal coordinates, respectively.

Because of its tendency to form a variety of stable hydrogen bonded networks, antamanide is an ideal candidate for testing the capacity of coherent nonlinear infrared (IR) methods to characterize hydrogen bond connectivity. A previous study used hydrogen bond induced redshifts to distinguish between folded and unfolded conformations of a  $\beta$ -heptapeptide.<sup>23</sup> To date, most nonlinear IR experiments were conducted on relatively small peptides, possessing less than ten units. Both vibrational energy level structure and relaxation dynamics of the prototypical monopeptide NMA were studied extensively by pump-probe<sup>20,24</sup> and photon-echo measurements.<sup>25</sup> Conformational fluctuations of NMA (and trialanine) were recently simulated using classical

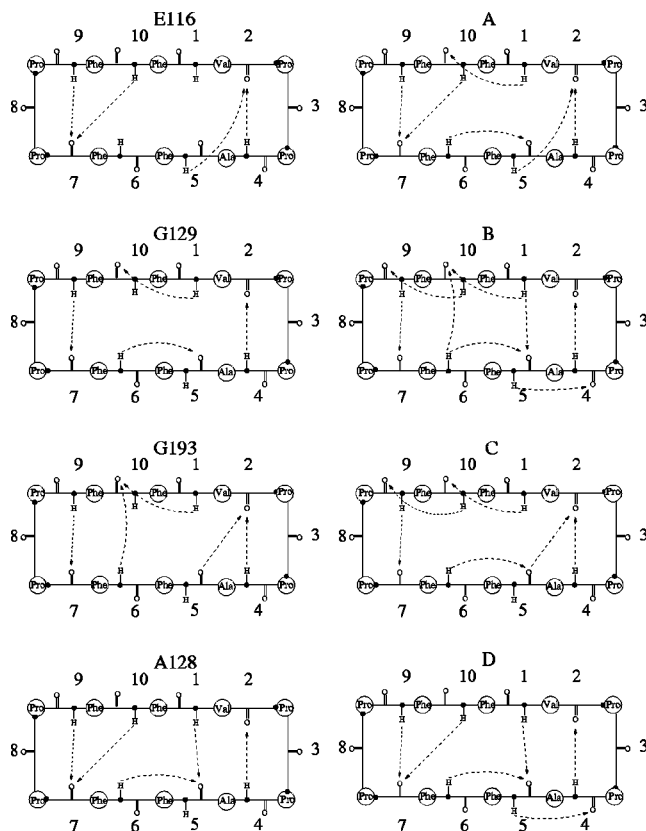


FIG. 2. Hydrogen bonding pattern of the four conformations (a) reported in Ref. 1 (left column) and (b) found here (right column) using the semiempirical AM1 Hamiltonian. Indices are assigned to all peptide planes, residues are denoted by standard abbreviations, and nitrogen atoms are represented by black dots. Hydrogen bonds obtained from the Kabsch-Sander criterion are conveyed by dashed arrows.

MD.<sup>26</sup> Polarization-sensitive photon-echo measurements were used to determine the angle between the transition dipoles of the amide I eigenmodes for both acetoprolin-NH<sub>2</sub><sup>27</sup> and trialanine.<sup>28</sup> In addition, isotopic editing strategies and *ab initio* calculations were employed to translate the experimentally determined transition dipole orientations of trialanine into the  $\phi$  and  $\psi$  Ramachandran angles describing the peptide backbone.<sup>28</sup> To that end, a least-squares procedure was used to fit a model Hamiltonian and known three-dimensional structure of a cyclic pentapeptide in solution to polarized pump-probe measurements, demonstrating the feasibility of extracting geometric information from experimental data for a molecule with more than two amide I modes. Most recently, temperature- and photo-induced structural changes were investigated for a  $\beta$ -hexapeptide<sup>29</sup> and a cyclic octapeptide,<sup>30</sup> respectively; the structural evolution of the  $\beta$ -peptide was monitored using IR pump-probe measurements, whereas polarized IR difference spectra were used to study the photo-induced dynamics of the octapeptide.

We have simulated the third order vibrational spectra of four conformations in the amide I region. These conformations are presented in Sec. II. The anharmonic vibrational exciton Hamiltonian and the methods used to obtain its parameters are described in Sec. III. Linear spectra are discussed in Sec. VI, whereas two-dimensional spectra and dis-

TABLE I. Parameters of the exciton Hamiltonian for the amide I modes ( $\text{cm}^{-1}$ ). The indices correspond to those presented in Fig. 2. The diagonal and off-diagonal elements represent the  $\Omega_\alpha$  and  $J_{\alpha\beta}$  of Eq. (2), respectively.

Row	Column	A	B	C	D	Row	Column	A	B	C	D
1	1	1769.8	1769.8	1769.8	1769.8	4	5	-3.1	-2.6	-1.2	-3.0
1	2	4.8	3.9	0.5	4.4	4	6	-0.1	1.1	0.0	0.1
1	3	-0.9	1.2	0.3	0.9	4	7	-0.5	-0.6	-0.2	-0.8
1	4	0.1	0.3	0.6	0.4	4	8	0.3	0.1	0.3	0.1
1	5	0.1	-3.2	1.5	-6.2	4	9	-0.1	-0.2	-0.2	-0.1
1	6	-1.1	2.0	1.0	2.2	4	10	-0.1	-0.3	-1.6	-0.3
1	7	-2.1	-0.2	-1.0	-2.1	5	5	1753.9	1758.1	1754.7	1755.4
1	8	0.8	0.6	0.8	0.5	5	6	10.3	0.7	-0.5	-0.7
1	9	-0.4	0.6	-0.9	1.4	5	7	-2.3	1.1	-1.2	3.5
1	10	7.5	0.8	1.6	-0.3	5	8	0.8	-0.6	0.8	-0.8
2	2	1756.3	1756.0	1754.8	1755.4	5	9	-0.1	-0.6	-0.2	-0.7
2	3	0.5	2.5	0.8	2.5	5	10	0.8	8.6	-5.9	-2.4
2	4	-5.3	-6.7	-5.3	-6.5	6	6	1769.8	1769.8	1769.8	1769.8
2	5	-6.5	-0.2	-6.4	-0.7	6	7	2.2	-0.5	2.5	-0.4
2	6	-1.6	-0.7	-2.2	-0.7	6	8	-2.2	1.4	-0.7	0.6
2	7	1.2	0.0	0.8	-0.0	6	9	-1.1	0.5	0.2	0.4
2	8	-0.1	0.3	-0.2	0.3	6	10	-3.5	-5.7	-4.3	1.4
2	9	-0.6	-0.7	-0.7	-0.4	7	7	1756.3	1755.1	1755.1	1757.2
2	10	-1.9	1.5	6.6	-1.5	7	8	-0.2	2.0	3.3	-0.2
3	3	1769.8	1769.8	1769.8	1769.8	7	9	-5.5	-6.2	-5.7	-5.7
3	4	9.1	-2.6	9.6	-2.6	7	10	-5.5	-2.2	-1.3	-6.4
3	5	1.9	2.2	1.8	2.0	8	8	1769.8	1769.8	1769.8	1769.8
3	6	0.9	0.5	0.8	0.7	8	9	5.4	-3.0	-3.1	8.4
3	7	-0.1	0.3	0.0	0.1	8	10	2.1	1.9	2.3	2.1
3	8	0.0	0.1	0.0	0.0	9	9	1769.8	1758.1	1756.2	1769.8
3	9	0.4	0.2	0.3	0.2	9	10	-2.6	-1.9	1.2	4.8
3	10	0.9	-0.8	-1.3	0.6	10	10	1753.3	1757.2	1761.0	1769.8
4	4	1769.8	1757.8	1769.8	1758.7	---	---	---	---	---	---

tinct features that differentiate the four conformers are given in Sec. V. Our results are finally discussed in Sec. VI.

## II. DOMINANT SECONDARY STRUCTURE CONFORMATIONS

Four dominant conformations were identified by Ernst *et al.*<sup>1</sup> (see Fig. 2, left column) by combining NMR results with a multiconformational search algorithm.<sup>1,10</sup> Distance constraints based on NMR cross-relaxation rates were incorporated into the CHARMM 22.0 force field<sup>31</sup> as semiparabolic energy terms. Subsequent geometry optimizations (*in vacuo*) were therefore driven towards minima consistent with the NMR-derived constraints. Conformations that survived certain selection criteria were then used to determine the most probable dynamic exchange pairs. This algorithm is outlined in Ref. 10. Another classical MD simulation of antamanide was performed in Ref. 32 starting with the x-ray crystal structure.

Our convention for assigning indices (Fig. 2) differs from that usually used for peptides.<sup>33</sup> We have assigned each peptide plane an index, which is most sensible for our purposes because each local amide I mode possesses amplitude on only a single unit. The first index refers to the peptide plane containing the amino group of the valine residue. The indices are then taken to increase around the ring in the direction of the adjacent proline residue.

In the present work we used a higher level theory: Energy minima were searched for using the AM1 semiempirical Hamiltonian and an optimization algorithm. GAUSSIAN 98<sup>34</sup>

was employed in all quantum-chemical calculations. Structural optimizations were carried out in two steps: (i) All atomic positions except for the hydrogen bonded oxygen and hydrogen atoms were optimized at the AM1 level; (ii) an unconstrained optimization was performed to search for minima with respect to all degrees of freedom. We started our optimizations at the four conformations reported in Ref. 1. Our A, B, C, and D conformations were found while attempting to optimize to the E116, G129, G193, and A128 conformations of Ref. 1, respectively.

The presence of a hydrogen bond was determined using the Kabsch-Sander criterion, which is based on the following expression for the hydrogen bond energy:<sup>35</sup>

$$E_{\text{KS}} = f q_1 q_2 \left( \frac{1}{d_{\text{ON}}} + \frac{1}{d_{\text{CH}}} - \frac{1}{d_{\text{CN}}} - \frac{1}{d_{\text{OH}}} \right), \quad (1)$$

where  $q_1 = 0.42e$ ,  $q_2 = 0.20e$ , and  $f = 1390 e^{-2} \text{ \AA} \text{ kJ/mol}$ .<sup>35</sup> Distances are measured with respect to the C=O of the hydrogen bond acceptor and N-H of the donor. Hydrogen bonds are considered to exist for all C=O/N-H pairs in which  $E_{\text{KS}} < -2.1 \text{ kJ/mol}$ .<sup>31</sup>

The two columns in Fig. 2 compare the hydrogen bonding patterns obtained for our AM1 conformers with those reported by Ernst *et al.*<sup>1</sup> Note that a different criterion was used in Ref. 1 to determine the presence of hydrogen bonds; a hydrogen bond was assumed to exist when the N-O distance is less than 3.5 Å and the N-H-O angle is larger than 105°. The relative free energies of our four conformations with the inclusion of zero-point energies and thermal popu-

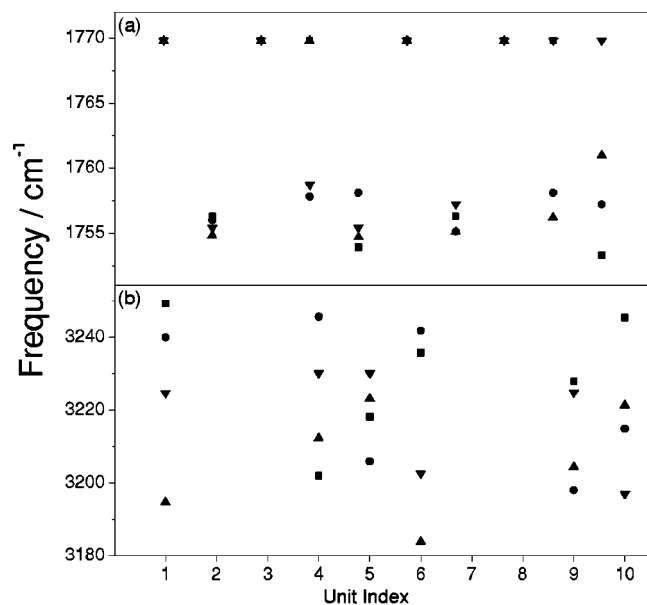


FIG. 3. (a) Vibrational frequencies of the local amide I calculated using Eq. (4). Frequencies of the amide A modes taken directly from the force constant output of an AM1 Hessian calculation. The four conformations are represented by the following symbols: A (squares); B (circles); C (triangle pointed up); D (triangle pointed down). Unit label indices are given in Fig. 2.

lation corrections at room temperature are A (0 kJ/mol), B (3.549 kJ/mol), C (6.245 kJ/mol), and D (15.501 kJ/mol). The relative conformational enthalpies reported in Ref. 1 are E116 (21 kJ/mol), G129 (0 kJ/mol), G193 (59 kJ/mol), and A128 (7 kJ/mol).<sup>31</sup>

### III. EXCITON DESCRIPTION OF THE AMIDE MODES

Our modeling of the amide I and A modes starts with identifying the relevant local amide modes (LAM)  $\{Q_\alpha\}$  residing on each peptide plane. Antamanide possesses ten local amide I modes, but only six local amide A modes due to the presence of four proline residues.

We assume the following expansion of the vibrational Hamiltonian in terms of these LAM:<sup>18</sup>

$$H = \frac{1}{2} \sum_{\alpha} (\Omega_{\alpha} - \Delta_{\alpha}) Q_{\alpha}^2 + \frac{1}{12} \sum_{\alpha} \Delta_{\alpha} Q_{\alpha}^4 + \sum_{\alpha < \beta} J_{\alpha\beta} Q_{\alpha} Q_{\beta}, \quad (2)$$

where  $\Omega_{\alpha}$  and  $\Delta_{\alpha}$  are the frequencies and anharmonicities of the LAM. The coupling with the radiation field is  $-\mu E(t)$  where the dipole operator is expanded to first order in  $Q_{\alpha}$

$$\mu = \sum_{\alpha} \mu_{\alpha} Q_{\alpha}, \quad (3)$$

and  $\mu_{\alpha}$  represents the dipole derivative with respect to  $Q_{\alpha}$ .<sup>18</sup> Each LAM is characterized by three parameters: a frequency  $\Omega_{\alpha}$ , an anharmonicity  $\Delta_{\alpha}$ , and a dipole derivative,  $\mu_{\alpha}$ . The LAM are harmonically coupled by the bilinear couplings  $J_{\alpha\beta}$ .

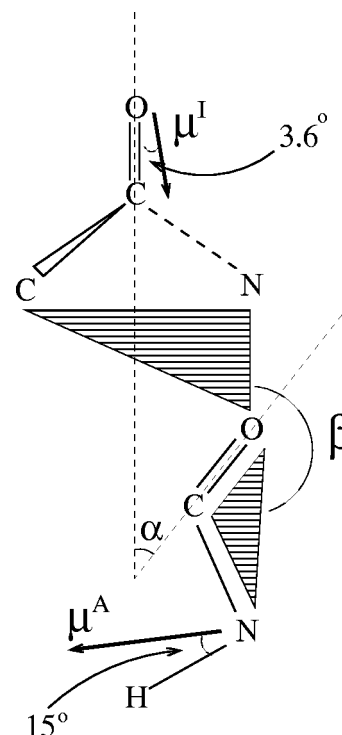


FIG. 4. Structural parameters used in our simulations, the  $\alpha$  coordinate of Table IV is the angle between the two vectors oriented along the C=O axes. The  $\beta$  coordinate is defined as the angle between the two planes: (i) a plane involving N, C', and O of the hydrogen bond acceptor; (ii) a plane defined by the atomic positions of C<sub>α</sub> and N of the donor along with O of the acceptor. The orientations of the local transition dipoles are shown for the amide I of the hydrogen bond donor.

### A. Parameters for the amide I band

We have assumed a single local amide I mode ( $Q_{\alpha}$ ) located on each peptide plane. These modes are delocalized over several internal coordinates associated with the peptide planes, but the precise composition of the local mode does not enter into the present simulation. DFT calculations of *trans*-NMA predict that the C'=O and C'-N stretches as well as the C<sub>α</sub>-C'-N and C'-N-H bends carry the most amplitude in the amide I normal mode. These coordinates were used to calculate anharmonic 3-level systems in Ref. 18 at the DFT level.

A B3LYP/6-31G\*\* normal mode analysis of *trans*-N-methylacetamide (NMA) was used to parametrize the amide I frequencies  $\Omega_{\alpha}^{\circ}$  of nonhydrogen bonded amide I modes (1769.8 cm<sup>-1</sup>). The same value of  $\Omega_{\alpha}^{\circ}$  was assigned to all bonds and the existence of a hydrogen bond was determined using Eq. (1). Local amide I frequencies were calculated as  $\Omega_{\alpha} = \Omega_{\alpha}^{\circ} + \Delta\Omega_{\alpha}$ , where

$$\Delta\Omega_{\alpha} = \alpha_H(2.6 - d_{OH}), \quad (4)$$

and  $\Delta\Omega_{\alpha}$  represents the amide I frequency shift determined by the hydrogen bond distance  $d_{OH}$ . The slope  $\alpha_H$  was set to  $-30 \text{ cm}^{-1}/\text{\AA}$ , producing a  $\sim 20 \text{ cm}^{-1}$  redshift for common hydrogen bond distances of 1.9–2.0 Å.<sup>35,36</sup> The resulting ten local amide I mode frequencies are given in Table I and displayed in Fig. 3.

The empirical formula [Eq. (4)] was used in lieu of calculating all of the frequencies explicitly to reduce computa-

TABLE II. Parameters of the exciton Hamiltonian for the amide A modes ( $\text{cm}^{-1}$ ).<sup>a</sup>

Row	Column	A	B	C	D	Row	Column	A	B	C	D
11	11	3224.7	3194.8	3240.0	3249.3	13	13	3230.1	3223.2	3206.0	3218.2
11	12	-0.4	-0.7	-0.3	-0.7	13	14	-0.9	-0.4	-1.0	-1.1
11	13	-0.8	-0.5	0.3	-0.7	13	15	-0.3	-0.1	-0.5	-0.1
11	14	-0.1	1.3	0.1	1.5	13	16	-1.0	0.1	-0.7	-0.1
11	15	-0.6	-0.2	-0.3	0.3	14	14	3202.6	3183.9	3241.8	3235.8
11	16	-1.5	-0.9	-0.7	0.3	14	15	-0.4	-0.9	-0.5	-0.5
12	12	3230.1	3212.4	3245.7	3202.0	14	16	-1.5	-0.8	0.0	-0.6
12	13	2.1	-0.7	1.8	-0.7	15	15	3224.8	3204.5	3198.0	3227.9
12	14	-0.5	0.0	-0.5	-0.3	15	16	2.0	-0.9	-1.3	1.1
12	15	-0.2	-0.1	-0.2	-0.1	16	16	3197.0	3221.4	3214.9	3245.4
12	16	-0.4	-0.1	-0.2	-0.2	---	---	---	---	---	---

<sup>a</sup>Same as Table I for the amide A modes.

tional cost. This should be sufficient for our goal of predicting nonlinear infrared signatures of different hydrogen bonded conformations. Improved parametrization could be based on an *ab initio* grid such as those presented for the amide I bilinear coupling coefficients ( $J_{\alpha\beta}$ ) in Refs. 17 and 37. This will be critical for MD simulations aimed at reproducing large-scale conformational changes among secondary structures, where many points along a trajectory need to be parametrized.

In our previous study we found the amide I anharmonicity to be relatively insensitive to hydrogen bonding.<sup>18</sup> We have therefore taken all local amide I modes anharmonicities to be  $15 \text{ cm}^{-1}$ , a value consistent with previous theoretical<sup>18</sup> and experimental work.<sup>20</sup> Transition dipole orientations were based on DFT calculations of NMA (and its dimers).<sup>18</sup> The local amide I dipole derivative was assumed to form an angle of  $3.6^\circ$  with respect to the C=O bond (points towards the amide bond) in the O=CN plane (see Fig. 4).

We used the results of Torii and Tasumi for the magnitude<sup>14</sup> ( $3.7 \text{ D \AA}^{-1} \text{ amu}^{-1}$ ) and position<sup>37</sup> of the transition dipoles. The transition dipole magnitudes of the amide I mode calculated for isolated NMA and its dimers at the B3LYP/6-31+G\*\* level are  $\sim 4.75$  larger than that of Ref. 14, which results in unphysical magnitudes for the bilinear coupling coefficients (see the next paragraph). This suggests a limitation of predicting exciton Hamiltonian parameters from calculations of isolated repeat units.

The bilinear coupling coefficients between amide I modes were calculated using a transition dipole coupling (TDC) model for nonadjacent neighbors.<sup>38,39</sup> Couplings between local amide I modes for covalently bonded units were taken from the *ab initio* grid reported in Ref. 37 and graciously provided to us by the authors; the coupling coefficient was defined as a function of the  $\phi$  and  $\psi$  dihedral angles for the peptide backbone (Ramachandran space).<sup>32</sup> This parametrization scheme was chosen because the TDC model does not accurately describe the interaction between nearest-neighbor amide I modes.<sup>37</sup>

## B. Parameters for the amide A band

We have represented the local amide A modes by a single coordinate, the N-H stretch, which is highly localized and only weakly coupled to neighboring modes.

Fundamental frequencies ( $\Omega_\alpha$ ) were taken directly from the AM1 force constants at the four equilibrium conformations (see Table II and Fig. 3). These could have been obtained from higher level DFT calculations for model molecules. However, it is not clear whether the highly environment-sensitive frequencies of the N-H stretch are adequately captured by these smaller model systems. Local amide A anharmonicities were calculated by cutting NMA dimers representing hydrogen bonded pairs of units out of the four AM1 optimized conformers. Force constants were then calculated to fourth order with respect to the N-H stretch coordinate at the B3LYP/6-31G\*\* level and used to parametrize the anharmonicities (see Table III). We found the AM1 level to be inadequate for calculating anharmonicities.

To reduce computational cost (avoid the explicit computation of the anharmonicity for all 24 hydrogen bonded pair of units) and characterize the sensitivity of the anharmonicity to specific structural coordinates, the amide A modes were grouped according to the values of three local coordinates selected to provide a clear picture for the orientations of the pairs peptide planes (see Fig. 4). Two of these coordinates are the hydrogen bond distance  $R_{\text{OH}}$  and the angle  $\alpha$  between the C=O bonds for hydrogen bonded pairs of peptide planes. The third coordinate ( $\beta$ ) is defined as the angle between two planes: (i) a plane involving N, C', and O of the hydrogen bond acceptor; (ii) a plane defined by the atomic positions of  $C_\alpha$  and N of the donor along with O of the acceptor. We found that the 24 hydrogen bonds (four conformations with six bonds each) could be classified into seven groups whose frequencies and (B3LYP/6-31G\*\*) anharmonicities are presented in Table IV.

The amide A anharmonicities were calculated explicitly

TABLE III. Local amide A anharmonicities ( $\text{cm}^{-1}$ ).

Unit <sup>a</sup>	A	B	C	D
1	34.3	34.3	30.3	32.3
2	33.9	33.6	33.9	33.6
3	37.5	31.1	32.2	31.1
4	34.3	32.3	34.3	34.3
5	33.9	33.6	33.6	33.9
6	32.3	31.1	34.3	32.2

<sup>a</sup>The unit indices correspond to those shown in Fig. 2.

TABLE IV. DFT transition frequencies for the amide A mode.

Subset <sup>a</sup>	R <sub>OH</sub>	$\alpha$	$\beta$	$\Omega$	$\Delta$
1	2.05	132.8	106.8	3342.1	34.3
2	2.10	161.7	33.8	3388.1	33.9
3	2.11	131.4	78.4	3398.3	33.6
4	2.15	100.9	52.6	3347.7	37.5
5	2.21	134.3	119.3	3405.8	31.1
6	2.33	97.5	35.0	3396.6	32.2
7	2.51	133.0	80.9	3432.8	32.3

<sup>a</sup>Bond lengths and angles are given in units of Å and degrees, respectively. Frequencies ( $\Omega$ ) and anharmonicities ( $\Delta$ ) are given in units of  $\text{cm}^{-1}$ . The coordinates  $\alpha$  and  $\beta$  are depicted in Fig. 4.

because they are more sensitive to hydrogen bonding than those of amide I.<sup>18</sup> However, the calculations in Ref. 18 were performed for relatively close hydrogen bond distances in helical structures ( $\sim 1.90$  Å), whereas the distances here are at least  $0.15$  Å longer and therefore less sensitive to local structure. All calculated anharmonicities reside in the  $30$ – $37.5$   $\text{cm}^{-1}$  range. The transition dipole magnitude ( $2.2$  D Å<sup>-1</sup> amu<sup>-1</sup>) was based on the relative experimental extinction coefficients<sup>40</sup> for the amide I and amide A modes and the absolute transition dipole magnitude for the amide I mode reported in Ref. 14. The amide A dipole derivative is taken to make an angle of  $15^\circ$  with the N–H bond in the

peptide plane and points to the carbonyl side of the N–H bond (see Fig. 4).<sup>18</sup>

Quadratic off-diagonal force constants obtained from semiempirical AM1 Hessian calculations were used to parametrize the couplings between local modes (N–H coordinates; see Table II). These were generally weak ( $< 2$   $\text{cm}^{-1}$ ) and therefore had little effect on the delocalization of the calculated eigenmodes. In addition, couplings between local amide I (approximated as the C=O coordinates) and amide A modes were taken from second-order AM1 force constants (see Table V). The amide I mode was considered as the C=O stretch in lieu of numerically differentiating with respect to a collective amide I coordinate. This is reasonable because the C=O stretch carries the most amplitude in this mode and is also the internal coordinate most strongly coupled to the N–H stretch by hydrogen bonds.

The coupling coefficients between hydrogen bonded N–H and C=O coordinates ( $\sim 10$   $\text{cm}^{-1}$ ) were much larger than between nonbonded pairs that are not part of the same peptide plane ( $< 1$   $\text{cm}^{-1}$ ), and therefore constitute a good measure of hydrogen bond connectivity. These parameters have little effect on the energy levels since they are much smaller than the frequency differences between the amide I and amide A modes. However, dynamical processes such as energy transfer between hydrogen bonded units that could be

TABLE V. Coupling coefficients between amide I and A modes ( $\text{cm}^{-1}$ ).<sup>a</sup>

Row	Column	A	B	C	D	Row	Column	A	B	C	D
1	11	-11.0	-10.5	-7.5	-8.8	6	11	-0.2	1.0	0.4	0.8
1	12	1.0	0.3	0.6	0.3	6	12	-1.0	-0.2	-0.8	-0.5
1	13	1.4	-0.5	1.3	-0.8	6	13	-3.5	-2.7	-3.3	-2.8
1	14	0.1	0.9	0.1	0.8	6	14	-12.4	-11.0	-10.4	-7.9
1	15	-1.0	-0.4	-0.8	-0.1	6	15	1.0	0.4	0.9	0.4
1	16	-3.4	-3.4	-2.9	-1.6	6	16	-7.7	-0.8	0.1	0.4
2	11	-2.2	-4.3	-4.9	-3.3	7	11	-1.3	-0.4	-0.8	-0.8
2	12	-6.2	-4.4	-3.3	-5.8	7	12	-0.1	-0.4	-0.1	-0.4
2	13	-9.5	0.4	-8.5	0.3	7	13	-0.4	-0.3	-0.8	0.0
2	14	-0.7	-0.4	-0.9	-0.7	7	14	-1.6	-4.9	-3.0	-4.3
2	15	-0.2	-0.4	0.0	-0.3	7	15	-8.3	-7.9	-10.7	-6.6
2	16	-0.3	-0.2	0.6	-0.5	7	16	-10.1	0.0	0.1	-8.3
3	11	-0.2	0.3	0.1	0.3	8	11	0.4	0.2	0.2	-0.1
3	12	-1.4	-1.7	-1.5	-2.3	8	12	0.1	0.1	0.2	0.1
3	13	-0.3	0.6	-0.5	0.7	8	13	0.2	-0.1	0.4	-0.1
3	14	0.3	0.0	0.3	0.2	8	14	-0.2	0.4	-0.1	0.1
3	15	0.2	0.1	0.2	0.1	8	15	-2.1	-2.6	-2.5	-2.2
3	16	0.3	-0.1	-0.1	0.1	8	16	-0.2	0.8	1.1	0.1
4	11	-0.3	-0.3	0.0	-0.1	9	11	0.4	0.8	0.6	0.4
4	12	-8.3	-10.0	-8.8	-14.2	9	12	-0.1	-0.1	-0.2	-0.1
4	13	1.0	-12.6	0.6	-17.3	9	13	-0.2	-0.1	-0.3	-0.2
4	14	0.2	0.8	0.4	1.0	9	14	-0.3	-0.2	-0.3	-0.1
4	15	-0.1	-0.1	-0.2	-0.1	9	15	-10.7	-12.6	-13.5	-10.7
4	16	-0.2	-0.2	-0.3	-0.3	9	16	1.4	-14.7	-18.1	1.4
5	11	-0.6	-5.3	0.2	-7.3	10	11	-16.8	-15.5	-8.5	1.6
5	12	-0.8	-3.7	-0.8	-5.1	10	12	-0.5	0.4	0.2	-0.5
5	13	-9.9	-8.1	-9.5	-11.0	10	13	-0.8	0.9	-4.6	-0.3
5	14	-15.5	-13.9	-17.4	-19.4	10	14	-0.8	-7.0	-0.3	0.1
5	15	-0.6	0.4	-0.8	0.3	10	15	-1.2	-4.2	-4.3	-1.3
5	16	-0.7	0.9	-0.8	0.6	10	16	-9.7	-9.7	-10.1	-6.5

<sup>a</sup>Same as Table I for  $\mathbf{J}_{\alpha\beta}$  between the amide I and A modes.

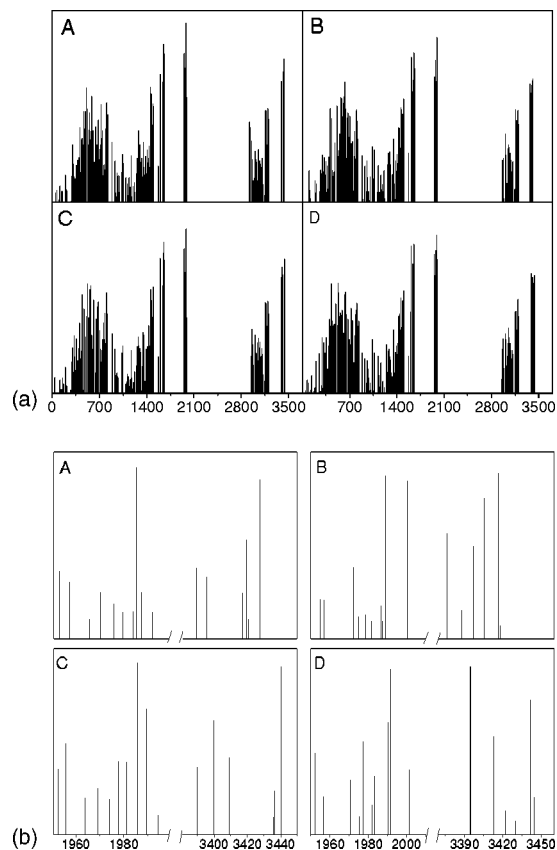


FIG. 5. (a) Harmonic linear infrared spectra (all  $3N-6$  coordinates) calculated using the AM1 semiempirical Hamiltonian for the four conformations shown in Fig. 2. (b) High-resolution spectra of panel (a) for the amide I and A regions.

detected by three pulse-echo<sup>36</sup> and pump-probe techniques are determined by these couplings.

#### IV. LINEAR INFRARED ABSORPTION

Absorption spectra resulting from harmonic normal mode analysis ( $3N-6$  coordinates) at the AM1 level are presented in Fig. 5. We focused on the amide I ( $1900-2010\text{ cm}^{-1}$ ) and A ( $3350-3450\text{ cm}^{-1}$ ) regions shown in Fig. 5(a). Higher resolution spectra of these two bands are given in Fig. 5(b). Compared to experiment,<sup>41</sup> the amide I frequencies are blueshifted by about  $300\text{ cm}^{-1}$ , whereas the amide A frequencies are only blueshifted by about  $100\text{ cm}^{-1}$ .

The anharmonic spectra were computed using the method outlined earlier.<sup>18,19</sup> Our basis of local amide modes consists of the ground state and the singly and doubly excited states. We have adopted the Heitler London approximation for the couplings  $J_{\alpha\beta}$  [Eq. (2)] and neglected matrix elements between manifolds with a different number of excitons. The single and double exciton blocks were then diagonalized separately and the spectra were computed using the eigenstates. Figure 6 shows the resulting linear infrared absorption for the four conformations in the amide I and A regions. The amplitude localization of the six amide A modes ( $Q_\alpha$ ) are represented by the N-H bonds shown in Fig. 2. To

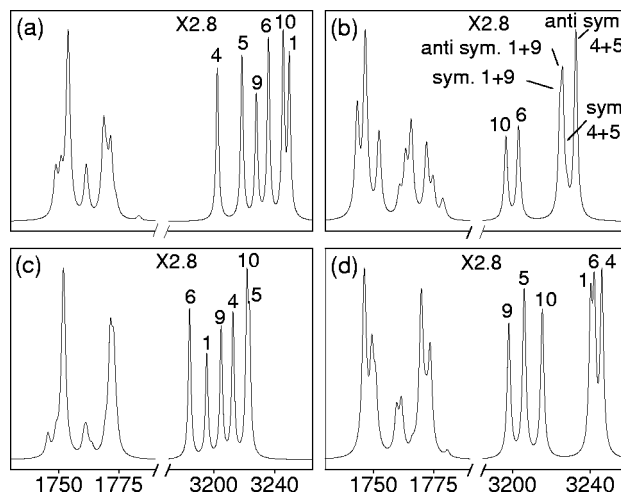


FIG. 6. Linear infrared spectra in the amide I and amide A regions for the four conformations as indicated (Fig. 2), calculated using the anharmonic vibrational Hamiltonian [Eq. (2)]. All spectra are normalized. Labels on the amide A peaks correspond to the unit indices of Fig. 2, and represent the localization of vibrational amplitudes.

optimally display the level structure, we assumed a small homogeneous linewidth of  $2\text{ cm}^{-1}$  for all transitions.

The amide A transitions are unresolved experimentally due to broadening caused by hydrogen bonding, whereas a few features are seen in the amide I region.<sup>41</sup> The frequencies and linewidths of the amide A band in nonhydrogen bonding solvents suggest that all amino groups are hydrogen bonded,<sup>41</sup> which is consistent with our calculations *in vacuo*.

The calculated amide A modes are highly localized, with over 95 % of the amplitude residing on single units for the B, C, and D conformations; delocalized symmetric and anti-symmetric stretching combinations that form in the A conformer are exceptions (see Fig. 6). The indices used to label the amide A transitions correspond to the unit indices shown in Fig. 2 and indicate localization of the vibrational amplitude associated with the peak. The change in these frequency orderings between different conformations reflects the relative hydrogen bonding strengths. However, experimental resolution of these transitions would be complicated by large homogeneous broadening, which is not included in our simulations.

In contrast to the amide A, the vibrational amplitudes of the amide I modes presented in Fig. 6 are delocalized over several units, prohibiting a strictly local interpretation. However, clear differences do exist, so this spectral range in conjunction with sufficiently detailed modeling could be useful for distinguishing different conformations.

Isotopic editing strategies can be used to spectrally isolate a subset of modes, and facilitate a real-space interpretation of the spectra. Figure 7 shows the linear spectra of an isotopic derivative of antamanide in the A-D conformations where the  $^{13}\text{C}$  isotope has been substituted for the carbonyl  $^{12}\text{C}$  on units 1, 5, 6, and 10 (see Fig. 2). These units were chosen because they participate in hydrogen bonding in all conformations. A frequency downshift of  $43.5\text{ cm}^{-1}$  was introduced in  $\Omega_\alpha$  for all labeled modes based on a DFT calculation for isolated NMA.<sup>18</sup> The amplitudes of the calculated

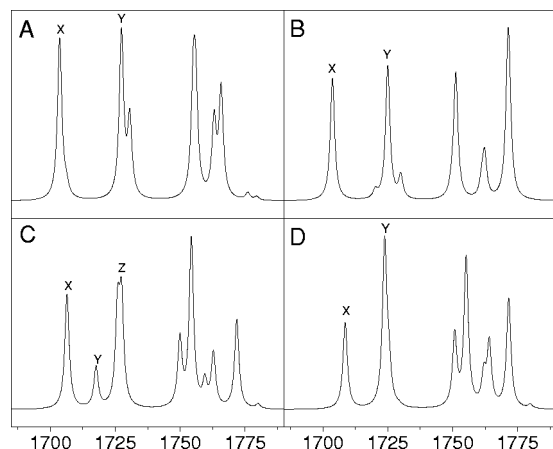


FIG. 7. Linear infrared spectra for an isotopomer in the four conformations as indicated (Fig. 2). Labels are placed on the most intense and resolvable peaks characterized by amplitude localization on the isotopically labeled units.

eigenmodes are dominated by these four units and the calculated frequencies and integrated intensities are presented in Table VI.

### V. THREE-PULSE PHOTON ECHOES

Multidimensional infrared signals are sensitive to the angles between transition dipoles of the coupled modes.<sup>42</sup> Consequently, their various tensor components,<sup>43</sup> which can be readily measured using different pulse polarization configurations, provide direct signatures of molecular geometry. Figures 8 and 9 show polarized three-pulse photon echo spectra for antamanide and its isotopomer, respectively. Calculations were performed in the snapshot limit; the incident pulses were taken to be impulsive in time and possessed uniform spectral intensity over the amide I region.<sup>44</sup> A homogeneous  $2\text{ cm}^{-1}$  linewidth was assumed for all transitions. Resonant terms in the response function were selected by applying the rotating wave approximation manually rather than by integration over pulse envelopes.<sup>44</sup> The  $\omega_1$  and  $\omega_3$  frequency axes correspond to the first and third time intervals in the pulse sequence, and the second interval was set to zero. The spectra were calculated using the sum over states expression<sup>44</sup> and orientational factors were incorporated using Eq. (13) of Ref. 42.

Figure 8 shows the photon echo spectra for each conformation in the ZZZZ polarization configuration. Peaks representing the strong transitions seen in the linear spectra (Fig. 6) as well as their doubly excited overtones and combination

TABLE VI. Calculated eigenmodes of the isotopomer of antamanide.

A	B	C	D
Frequency (intensity) <sup>a</sup>			
1703.6 (0.97)	1703.7 (0.91)	1706.4 (1.00)	1708.6 (0.53)
1706.2 (0.06)	1720.2 (0.06)	1717.6 (0.35)	1723.8 (1.00)
1727.4 (0.00)	1725.0 (1.00)	1725.9 (0.80)	1725.4 (0.22)
1730.6 (0.47)	1730.0 (0.17)	1727.4 (0.89)	1729.4 (0.01)

<sup>a</sup>The intensities represent the squares of the transition dipoles and are normalized to the maximum value.

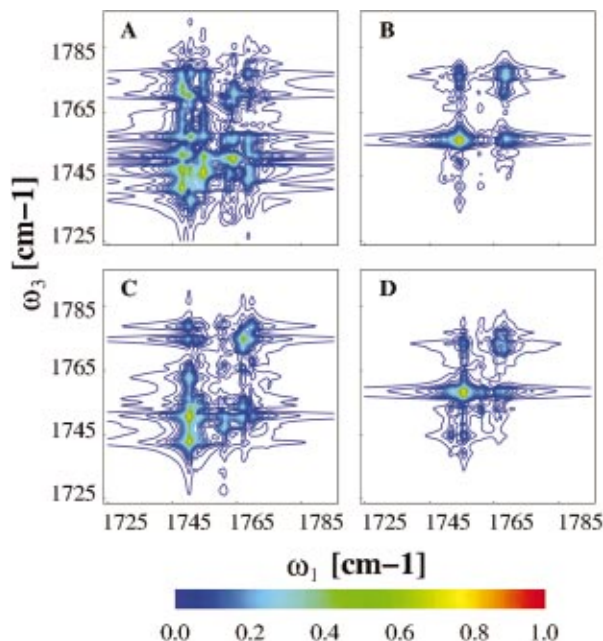


FIG. 8. (Color) Three-pulse photon echo spectra for the four conformations of antamanide as indicated. All spectra are calculated for parallel polarizations of the four fields, setting the second time interval to zero. The spectra are normalized to the peak intensity of the B conformer.

bands are clearly visible. Liouville space paths that involve only singly excited (fundamental) transitions of one mode generate diagonal peaks ( $-\omega_1 = \omega_3$ ), whereas pathways accessing their overtones are shifted down the  $\omega_3$  axis by the anharmonicities.<sup>45,46</sup> Cross peaks corresponding to singly excited states of two different modes are seen at  $(-\omega_1, \omega_3) = (-\Omega_a, \Omega_b)$ , where the indices  $a$  and  $b$  denote the two modes. Transitions involving the modes  $a$  and  $b$  combination bands are shifted down the  $\omega_3$  axis from  $(-\Omega_a, \Omega_b)$  by the anharmonicity of the band  $\Delta_{ab}$ , and appear at  $(-\Omega_a, \Omega_b - \Delta_{ab})$ . These features are clearly seen in Fig. 8, but may be difficult to resolve experimentally due to larger line broadening in these congested bands. Furthermore, even with satisfactory resolution these eigenmodes are delocalized, complicating the prediction of a robust nonlinear IR signature of structure. We therefore turn to the isotopic derivatives described in Sec. IV.

Figure 9 shows three-pulse photon echo spectra for the A–D conformations of the isotopomer of antamanide in the amide I region for both ZZZZ and ZXXZ lab frame polarizations of the four fields (in these indices time increases from right to left). Peak labels are the same as in Fig. 7. The two most intense peaks are labeled for the A, B, and D conformations, whereas three peaks are labeled for conformation C because they are relatively well resolved and of comparable intensity.

For conformation A, the ZXXZ cross-peak intensities are only reduced by about 10% compared to ZZZZ because the angle between the  $1703.6$  (mostly units 5 and 6) and  $1727.4\text{ cm}^{-1}$  (mostly units 1 and 10) modes is  $156^\circ$ ; no attenuation would be seen for parallel transition dipoles. The modes of this conformer have anharmonicities of about

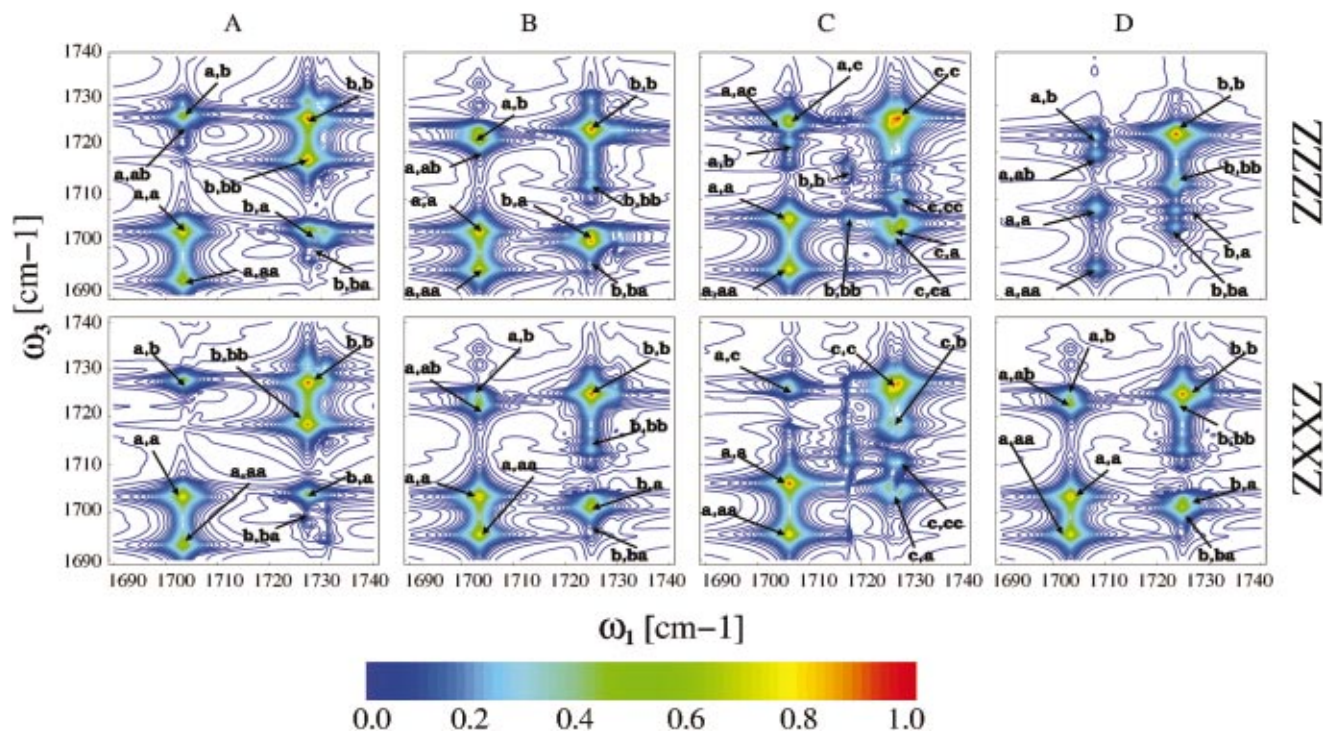


FIG. 9. (Color) Three-pulse photon echo spectra for an isotopomer of antamanide. The ZZZZ and ZXXZ polarized pulse configurations of the four conformers are presented in the first and second row, respectively. The A, B, C, and D conformers are shown in rows 1, 2, 3, and 4. The peak intensities of all the ZZZZ spectra are normalized to 1. The ZXXZ peak intensities are normalized to the peak intensity of the ZZZZ spectrum for the same conformer.

$10 \text{ cm}^{-1}$ . Also, the cross-peak anharmonicities are too small to be resolved ( $< 1 \text{ cm}^{-1}$ ).

The attenuation of the cross-peak intensities is easily interpreted for conformation B because the two strongest peaks (a and b) are composed of single modes. These  $1703.7$  and  $1725.0 \text{ cm}^{-1}$  peaks are predominantly localized on units 5/10 and 1/6, respectively. The transition dipole orientations for these modes differ by  $36^\circ$ , resulting in an intensity reduction of about 25% in the ZXXZ pulse configuration. Each of the modes has  $\sim 8 \text{ cm}^{-1}$  anharmonicity, whereas the cross-peak anharmonicities are less than  $1 \text{ cm}^{-1}$ .

Three strong and relatively well-resolved modes are calculated for the C conformer, making it the most easily distinguishable from the others in the linear spectra. The  $1706.4$ ,  $1717.6$ ,  $1725.9$ , and  $1727.4 \text{ cm}^{-1}$  peaks are mostly localized on units 5/10, 5/10, 1/6, and 1/6, respectively. However, two modes of approximately equal intensities are calculated near  $1726 \text{ cm}^{-1}$ . The ratio of the a and c band

cross-peak intensity to the maximum peak intensity is reduced by 20% under the ZXXZ polarization condition compared to that of ZZZZ.

For conformation D, the ZXXZ cross-peak intensities are reduced by  $\sim 30\%$  compared to ZZZZ. This is due to the relative orientations of the transition dipoles for the  $1723.8$  and  $1725.4 \text{ cm}^{-1}$  peaks (both labeled as b) compared to that of the  $1708.6 \text{ cm}^{-1}$  transition (labeled as a); these are predominantly localized on units 1/6/10 ( $1723.8$  and  $1725.4 \text{ cm}^{-1}$ ) and 5 ( $1708.6 \text{ cm}^{-1}$ ), respectively. The angles between the four lowest frequency peaks are given in Table VII. As in conformation C, the modes have anharmonicities of about  $12 \text{ cm}^{-1}$ . In addition, only this conformer exhibits resolvable anharmonicities ( $3 \text{ cm}^{-1}$ ) for its cross peaks.

## VI. DISCUSSION

We found the amide A frequencies to be sensitive to local structure and conformation. In addition, these modes are highly localized, facilitating a local interpretation of spectral features. However, these transitions are not resolved experimentally due to large homogeneous broadening ( $\sim 60 \text{ cm}^{-1}$  in  $\text{CHCl}_3$ <sup>41</sup>). Isotopic labeling strategies in the amide I region could help distinguish the various conformers. Predictions of IR features for the amide A band require more information regarding the frequency fluctuations of these modes which can be obtained from a molecular dynamics simulation. Isotopic substitution resulted in the spectral isolation of a subset of transitions, pinpointing distinct differences in the nonlinear IR spectra for four conformations.

TABLE VII. Calculated angles between transition dipoles for an isotopomer of antamanide.<sup>b</sup>

Mode <sup>a</sup>	Mode <sup>a</sup>	A	B	C	D
1	2	65.7	124.7	102.0	123.7
1	3	156.0	36.0	37.1	101.6
1	4	52.6	119.9	140.9	29.0
2	3	115.8	95.8	118.1	74.1
2	4	115.7	87.3	70.0	124.2
3	4	127.6	101.9	111.4	130.6

<sup>a</sup>The mode indices are assigned in the order of increasing energy.

<sup>b</sup>All angles are given in units of degrees.

Coherent third-order techniques should be especially useful for distinguishing conformations A, B, and D because their linear spectra are so similar; experimental spectra are sure to exhibit broader transitions, making conformational characterization based on linear spectra infeasible. The most accessible features are the anharmonicities and the relative intensities of cross peak for different polarization configurations. Although these features may not be simply interpreted by inspection, due to the delocalization of the amide I modes, sufficiently detailed models and isotopic editing strategies should provide solid predictions that can be easily compared to measurements. Furthermore, computed parameters may be used to constrain empirical fitting procedures, so that realistic physical parameters can be optimally extracted from measurements. However, the best strategy for obtaining these parameters is still an open problem.

The highly anharmonic amide A mode should be useful for investigating hydrogen bonding patterns because of its strong coupling to local amide I modes with which it is hydrogen bonded. These couplings may be studied using, e.g., two-color pump-probe experiments in which the amide A is pumped and amide I is probed; the coupling between amide I and A modes is so small compared to the frequency difference between the amide I and A modes that it is not easily extracted from all nonlinear experiments (the anharmonicity of the amide I+A combination band is  $<1\text{ cm}^{-1}$ ). A MD simulation will therefore be required to calculate the fluctuations in the amide I to A coupling elements before the energy transfer between these modes can be calculated. Such simulations would also allow solvent-induced relaxation and line broadening mechanisms to be included.

## ACKNOWLEDGMENTS

The support of NIH Grant GM59230-01A2 and NSF Grant CHE-0132571 is gratefully acknowledged. We wish to thank Jens Dreyer and Wei Zhuang for most useful discussions. We also wish to thank Professor Rafael Brüschweiler for providing the molecular coordinates of Ref. 1 and Professor Hajime Torii for providing the *ab initio* grid of bilinear coupling coefficients reported in Ref. 22.

- <sup>1</sup>M. Blackledge, R. Brüschweiler, J. Griesinger, J. Schmidt, P. Xu, and R. Ernst, *Biochemistry* **32**, 10960 (1993).
- <sup>2</sup>H. Kessler, A. Müller, and K.-H. Pook, *Liebigs Ann. Chem.* **1989**, 903.
- <sup>3</sup>C. Kessler, H. Griesinger, J. Lautz, A. Müller, W. van Gunsteren, and H. Berendsen, *J. Am. Chem. Soc.* **110**, 3393 (1988).
- <sup>4</sup>H. Kessler, W. Bermel, A. Müller, and K.-H. Pook, in *The Peptides*, edited by V. Hruby (Academic, Orlando, 1985), Vol. 7.
- <sup>5</sup>Z. Madi, C. Griesinger, and R. Ernst, *J. Am. Chem. Soc.* **112**, 2908 (1990).
- <sup>6</sup>J. Peng, C. Schiffer, P. Xu, W. van Gunsteren, and R. Ernst, *J. Biomol. NMR* **8**, 453 (1996).
- <sup>7</sup>T. Bremi, R. Brüschweiler, and R. Ernst, *J. Am. Chem. Soc.* **119**, 4272 (1997).

- <sup>8</sup>T. Bremi and R. Brüschweiler, *J. Am. Chem. Soc.* **119**, 6672 (1997).
- <sup>9</sup>T. Wieland and H. Faulstich, *Crit. Rev. Biochem.* **1978**, 185.
- <sup>10</sup>R. Brüschweiler, M. Blackledge, and R. Ernst, *J. Biomol. NMR* **1**, 3 (1996).
- <sup>11</sup>D. Patel, *Biochemistry* **12**, 667 (1973).
- <sup>12</sup>W. Bürgermeister, T. Wieland, and R. Winkler, *Eur. J. Biochem.* **44**, 311 (1974).
- <sup>13</sup>S. Krimm and J. Bandekar, *J. Adv. Protein Chem.* **38**, 181 (1986).
- <sup>14</sup>H. Torii and M. Tasumi, *J. Chem. Phys.* **96**, 3379 (1992).
- <sup>15</sup>A. C. Scott, *Phys. Rep.* **217**, 1 (1992).
- <sup>16</sup>R. Kopelman, in *Excited States*, edited by E. C. Lim (Academic, New York, 1975), Vol. 2.
- <sup>17</sup>J.-H. Choi, S. Ham, and M. Cho, *J. Chem. Phys.* **117**, 6821 (2002).
- <sup>18</sup>A. Moran, S.-M. Park, J. Dreyer, and S. Mukamel, *J. Chem. Phys.* **118**, 3651 (2003).
- <sup>19</sup>A. Moran, J. Dreyer, and S. Mukamel, *J. Chem. Phys.* **118**, 1347 (2003).
- <sup>20</sup>P. Hamm, H. Lim, and R. Hochstrasser, *J. Phys. Chem. B* **102**, 6123 (1998).
- <sup>21</sup>G. Chaban, J. Jung, and R. Gerber, *J. Chem. Phys.* **111**, 1823 (1999).
- <sup>22</sup>S. Gregurick, G. Chaban, and R. Gerber, *J. Phys. Chem. A* **106**, 8696 (2002).
- <sup>23</sup>S.-M. Park, C. Scheurer, and S. Mukamel, in *Femtochemistry and Femtobiology: Ultrafast Dynamics in Molecular Science*, edited by A. Douhal (World Scientific, Singapore, 2002).
- <sup>24</sup>S. Woutersen, R. Pfister, P. Hamm, Y. Mu, D. Kosov, and G. Stock, *J. Chem. Phys.* **117**, 6833 (2002).
- <sup>25</sup>M. Zanni, M. Asplund, and R. M. Hochstrasser, *J. Chem. Phys.* **114**, 4579 (2001).
- <sup>26</sup>S. Woutersen, R. Pfister, Y. Mu, D. Kosov, and G. Stock, *J. Chem. Phys.* **117**, 6833 (2002).
- <sup>27</sup>M. Zanni, S. Gnanakaran, J. Stenger, and R. Hochstrasser, *J. Phys. Chem. B* **105**, 6520 (2001).
- <sup>28</sup>S. Woutersen and P. Hamm, *J. Phys. Chem. B* **104**, 11316 (2000).
- <sup>29</sup>P. Hamm, S. Woutersen, and M. Rueping, *Helv. Chim. Acta* **85**, 3883 (2002).
- <sup>30</sup>J. Bredenbeck, J. Helbing, T. Schrader, W. Zinth, C. Renner, R. Behrendt, L. Moroder, J. Wachtveitl, and P. Hamm, *PNAS* (2003).
- <sup>31</sup>B. Brooks, R. Bruccoleri, B. Olafsen, D. States, S. Swaminathan, and M. Karplus, *J. Comput. Chem.* **4**, 187 (1983).
- <sup>32</sup>R. Brüschweiler, B. Roux, M. Blackledge, C. Griesinger, M. Karplus, and R. R. Ernst, *J. Am. Chem. Soc.* **114**, 2289 (1992).
- <sup>33</sup>T. Creighton, *Proteins: Structures and Molecular Properties* (Freeman, New York, 1993).
- <sup>34</sup>M. J. Frisch, G. W. Trucks, H. B. Schlegel *et al.*, GAUSSIAN 98, Revision A.9, Gaussian, Inc., Pittsburgh, PA (1998).
- <sup>35</sup>W. Kabsch and C. Sander, *Biopolymers* **22**, 2577 (1983).
- <sup>36</sup>C. Scheurer, A. Piryatinski, and S. Mukamel, *J. Am. Chem. Soc.* **123**, 3114 (2001).
- <sup>37</sup>H. Torii and M. Tasumi, *J. Raman Spectrosc.* **29**, 81 (1998).
- <sup>38</sup>S. Krimm and Y. Abe, *Proc. Natl. Acad. Sci. U.S.A.* **69**, 2788 (1972).
- <sup>39</sup>W. Moore and S. Krimm, *Proc. Natl. Acad. Sci. U.S.A.* **72**, 4933 (1975).
- <sup>40</sup>B. Lal and L. Nafie, *Biopolymers* **21**, 2161 (1982).
- <sup>41</sup>V. Ivanov, A. Miroshnikov, N. Abdullaev, L. Senyavina, S. Arkhipova, N. Uvarova, K. Khalilulina, V. Bystrov, and Y. A. Ovchinnikov, *Biochem. Biophys. Res. Commun.* **42**, 654 (1971).
- <sup>42</sup>R. M. Hochstrasser, *Chem. Phys.* **266**, 273 (2001).
- <sup>43</sup>S. Popov, Y. Svirko, and N. Zheludev, *Susceptibility Tensors for Nonlinear Optics* (Institute of Physics, London, 1995).
- <sup>44</sup>S. Mukamel, *Principles of Nonlinear Optical Spectroscopy* (Oxford University Press, New York, 1995).
- <sup>45</sup>S. Woutersen and P. Hamm, *J. Phys.: Condens. Matter* **14**, 1035 (2002).
- <sup>46</sup>J. Dreyer, A. Moran, and S. Mukamel, *J. Chem. Phys.* (to be published).